Ballistic transport in InSb/InAlSb antidot lattices

Hong Chen, J. J. Heremans,[a] and J. A. Peters
Department of Physics and Astronomy, and the Nanoscale and Quantum Phenomena Institute, Ohio University, Athens, Ohio 45701

N. Goel, S. J. Chung, and M. B. Santos
Department of Physics and Astronomy, and Center for Semiconductor Physics in Nanostructures, The University of Oklahoma, Norman, Oklahoma 73019

(Received 8 December 2003; accepted 3 May 2004; published online 17 June 2004)

We investigate magnetotransport properties of antidot lattices fabricated on high-mobility InSb/InAlSb heterostructures. The temperature dependencies of the ballistic magnetoresistance peaks due to the antidot lattice are studied, and compared with mobility and density data over the same temperature range. A scattering time particular to antidot lattices is deduced, with a linear dependence on temperature between 0.4 and 50 K, attributed to acoustic phonon scattering. The mobility does not vary substantially over this temperature range, whereas above ~60 K a quadratic dependence of inverse mobility on temperature is noticed, attributed to optical phonon scattering. The very weak temperature dependence of the width of the ballistic magnetoresistance peaks indicates negligible thermal smearing for electrons in the InSb quantum well, a result of the small electron effective mass. © *2004 The American Institute Physical*. [DOI: 10.1063/1.1764945]

The transport properties of two-dimensional electron systems (2DESs) on which a periodically modulated potential is imposed, reveal valuable information about electron motion and scattering mechanisms, and have been previously utilized to explore mesoscopic transport, predominantly in GaAs/AlGaAs heterostructures. If the 2DES is deeply modulated, such that the potential maxima exclude the electrons from their vicinity, an antidot lattice results.[1] Antidot lattices in turn have proven valuable model systems to study phenomena ranging from transport properties to chaotic dynamics and quantum interference phenomena, and have been used as demonstration platforms for new lithographic techniques and materials systems.[2–4] In this work, we study the transport properties of antidot lattices fabricated on InSb/InAlSb heterostructures. InSb has attracted recent interest due to the high mobility that can be achieved particularly in heterostructures, and due to a strong spin–orbit interaction that can find applications in novel spin–electronic devices.[5] Yet, until recently,[6] no studies existed of the mesoscopic transport properties in InSb.

Our samples are fabricated from *n*-type InSb/InAlSb heterostructures grown on GaAs substrates by molecular beam epitaxy.[5] Electrons reside in a 20-nm-wide InSb well flanked by $In_{0.91}Al_{0.09}Sb$ barrier layers. The electrons are provided by Si δ-doped layers on both sides of the well, separated from the 2DES in the well by 30 nm spacers. A third Si doped layer closed to the heterostructure surface provides electrons to the surface states. The material as grown yields a mobility $\mu = 159\,000$ cm^2/V s, and two-dimensional density $N_s = 2.3 \times 10^{11}$ cm^{-2}, at a temperature $T = 0.4$ K, resulting in a mobility mean-free-path of ~1.3 μm. After patterning a Hall bar by photolithography and deep wet chemical etching, the antidot lattice was produced by standard electron beam lithography and wet etching, using PMMA as an etching mask. The lower inset in Fig. 1 shows an optical micrograph of the antidot lattice, with dimensions 120 μm $\times$ 50 μm, and lattice period 0.8 μm. The diameter of the dots is controlled predominantly by lateral etching, and amounts here to about 0.5 μm. Samples were fabricated with lattice periods of either 0.8 or 1.0 μm. In order to compare the transport coefficients between antidot lattices and the unpatterned 2DES, a separate Hall bar sample was also fabricated from the same InSb/InAlSb material. The 2DES density in the Hall bar could be adjusted by means of a metal gate on top of the heterostructure.

Four-contact measurements of the longitudinal resistance, R_{XX}, of the antidot lattice were performed at variable T, ranging from 0.4 to 50 K using standard lock-in techniques. The magnetic field (B) is applied perpendicularly to the 2DES. As shown in Fig. 1, strong Shubnikov–de Haas oscillations appear at B above 1 T, while at low field two

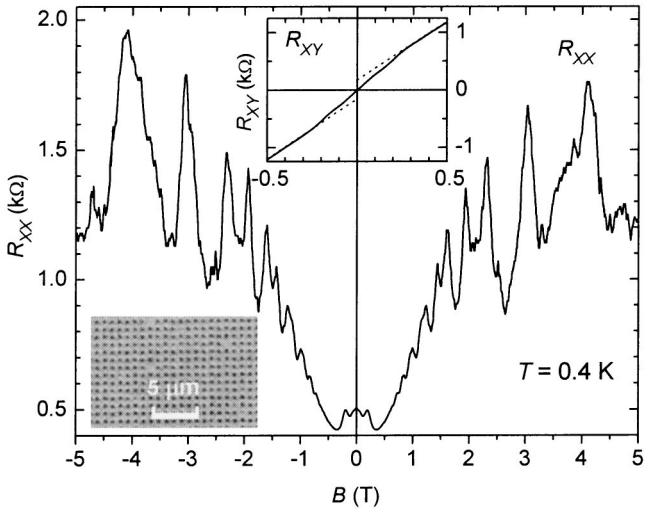

FIG. 1. Longitudinal magnetoresistance R_{XX} at $T = 0.4$ K. Low B: ballistic features due to antidots; high B: Shubnikov–de Haas oscillations. Upper inset: Hall resistance, R_{XY}, of the antidot lattice. The dashed lines are the linear extensions of R_{XY} from the regions of $B > 0.3$ T and $B < -0.3$ T. Lower inset: an optical micrograph of the antidot lattice.

[a]Electronic mail: heremans@helios.phy.ohiou.edu

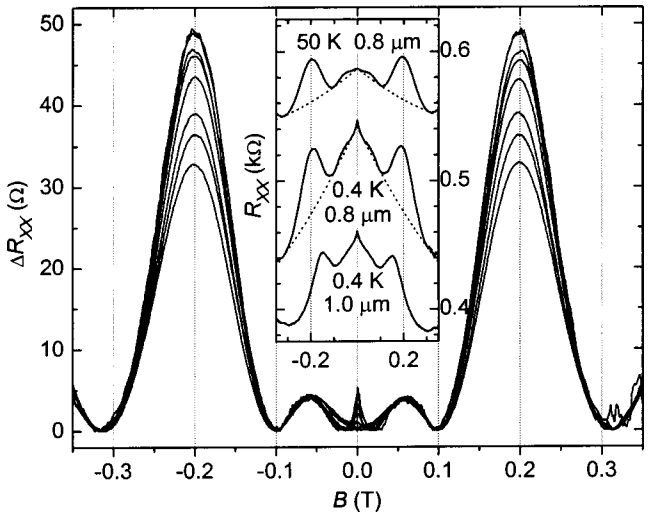

FIG. 2. Ballistic transport peaks, after subtracting a quadratic background, at different temperatures—from top to bottom: 0.4, 2.0, 5.0, 10, 20, 32, 40, and 50 K. Inset: low field R_{XX} of the 0.8 μm antidot lattice at 0.4 K and 50 K, with their background fits shown as dotted lines, as well as R_{XX} of the 1.0 μm lattice at 0.4 K.

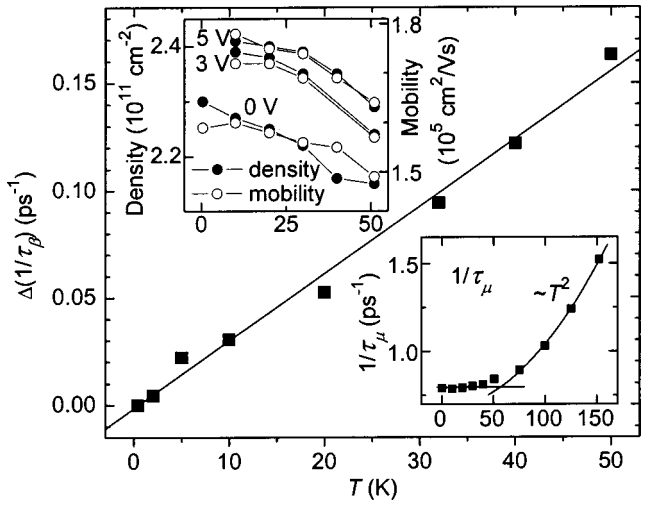

FIG. 3. Linear T dependence of the ballistic scattering rate $\Delta(1/\tau_\beta)$ as defined in the text. Lower inset: mobility scattering rate, $1/\tau_\mu$, on the unpatterned Hall bar at zero gate voltage, vs T. Upper inset: carrier density and mobility of the unpatterned Hall bar at gate voltages of 0, 3, and 5 V vs T.

ballistic transport peaks near $B=\pm 0.2$ T are observed. Detailed low-field magnetoresistance traces are contained in Fig. 2. The inset in Fig. 2 shows R_{XX} at the temperature extremes of our measurement, 0.4 and 50 K, for a lattice of 0.8 μm period, as well as R_{XX} at 0.4 K for a lattice of 1.0 μm period. Besides two strong peaks near $B=\pm 0.2$ T, two weak shoulders near ±0.06 T are observed on top of a negative magnetoresistance background. To extract the signals due to the features at ±0.06 and ±0.2 T, second-order polynomials (dotted lines in the inset of Fig. 2) were employed to fit the negative magnetoresistance on both positive and negative sides of B for the lattice of 0.8 μm period. The values of R_{XX} after background subtraction, ΔR_{XX}, are plotted in Fig. 2 for T ranging from 0.4 to 50 K. The figure shows strong maxima, $P1$, at ±0.20 T, and secondary maxima, $P2$, near ±0.056 T. The features represent the well-known commensurability maxima due to the correlation between the array parameters and the electron cyclotron orbit, a hallmark of ballistic transport.[1,2] The maxima still clearly appear at $T=50$ K, demonstrating the presence of ballistic transport at least up to this temperature. The maxima at ±0.20 T originate from ballistic electron trajectories encircling one antidot.[2] Indeed, using the carrier density of the InSb/InAlSb material at 0.4 K, $N_s=2.3\times 10^{11}$ cm^{-2}, a classical calculation yields an orbit diameter of 0.79 μm at $B=0.2$ T, matching the period of the antidot lattice, 0.8 μm. For the comparative sample with 1.0 μm lattice period, equivalent ballistic peaks appear at ±0.16 T (Fig. 2 inset) corresponding to an orbit diameter of 0.99 μm, again matching the period. In the semiclassical pinball model,[1,2] the magnetoresistance peak corresponding to this orbit can be explained by the assumption of a classical cyclotron orbit pinned around one antidot. The same calculation yields a diameter of 2.8 μm for the secondary maxima $P2$, at $B=0.056$ T, attributable to a circular orbit covering approximately nine antidots (0.8 μm period sample). Similar results concerning higher order maxima have been reported in InAs/GaSb antidot lattices.[7] It is well known, however, that the maxima can only be clearly identified with circular cyclotron orbits in the case of orbits encircling on antidot, whereas higher-order maxima result from more complex chaotic trajectories.[2,8] In our samples moreover, whereas the mean free path of ~1 μm is sufficient to support ballistic orbits around a single antidot, the 8.8 μm circumference implied by the 2.8 μm cyclotron diameter indicates that $P2$ requires more complete theoretical treatments invoking chaotic trajectories for the higher order peaks.[8] Interestingly, $P1$ and $P2$ also feature qualitatively different temperature dependencies. When T increases from 0.4 K to 50 K, the amplitude of $P1$ drops ~33%, while $P2$ stays almost unchanged. ΔR_{XX} also presents a small sharp peak around $B=0$, which disappears at higher T. This maximum appears in various mesoscopic geometries presently under study on InSb 2DESs, and is due to localization.[9]

The upper inset of Fig. 1 contains the Hall resistance, R_{XY}, of the antidot lattice sample, versus B. Deviations from linear behavior are observed between ±0.3 T, in the region of the ballistic maxima in R_{XX}. The modified Drude picture, known as the pinball model, that has emerged for transport in antidot lattices, predicts a reduction in the density of carriers participating in transport, and hence an increase in the slope of R_{XY}, at the commensurate magnetic fields and explains our observations.[1,2]

The value of B where the maximum $P1$ occurs is proportional to $N_S^{1/2}$. N_S drops by ~6% from 0.4 to 50 K, as shown in the upper inset of Fig. 3. The drop in turn leads to a change of ~3%, or ~6 mT in peak position—an undetectable amount. Hence, Fig. 2 does not show a noticeable shift in the position of $P1$ as the temperature increases. Figure 2 also reveals that the width of $P1$ remains nearly unchanged versus T. Since the peak width is determined by the thermal spread Δk_F in the Fermi wave vector, k_F,[3] such constancy of the width of $P1$ indicates a small thermal spread Δk_F. Analysis reveals that for a fixed N_s, $\Delta k_F/k_F \sim m^*(k_B T)$, where m^* denotes the electron effective mass and k_B the Boltzmann constant. The negligible thermal spread Δk_F and hence the reduced dependence on T of the peak width result from the small electron effective mass in InSb ($m^*=0.014\, m_0$ where m_0 represents the free electron mass). The small effective mass in InSb hence aids the observation of ballistic transport at high temperatures.

Figure 3 contains T-dependent data extracted for both the antidot sample and an unpatterned Hall bar with a top gate (used to change the carrier density). Above ~70 K, the top gate utilized on a separate Hall bar lost its ability to modify N_S, and substantial gate leakage currents appeared, indicating a lack of confinement of the 2DES, and the appearance of parallel conductance channels. We have therefore limited part of the data displayed over T in Fig. 3 to the range $0.4\ \mathrm{K} < T < 51\ \mathrm{K}$. The mean-free-path, calculated from μ and N_S on the gated Hall bar, ranged from 1.26 μm at 0.4 K to 1.14 μm at 51 K at zero gate voltage, a drop of only 10%. The maxima $P1$ are reduced by ~33% over this temperature range. It is well known from ballistic transverse magnetic focusing experiments[10,11] and from ballistic antidot experiments[3] that the amplitudes of ballistic magnetotransport signals depend exponentially on the ratio of the length of the ballistic orbit (e.g., for transverse magnetic focusing, the distance traveled between the injector and collector contacts), to a characteristic decay length. This decay length is experimentally not identical to the mobility mean-free-path, since ballistic experiments may experience an increased sensitivity to small-angle scattering (to which μ as an average property is not sensitive).[10–12] Hence the scattering time derived from the decay length addresses different scattering phenomena than the mobility scattering time, and it is of interest to compare the temperature dependence of both in the unexplored Isb/InAlSb system. The maxima $P1$ correspond to a cyclotron orbit pinned around one antidot. Hence (following Ref. 3), we replace the ratio of ballistic orbit length to characteristic decay length by $2\pi/\omega_c\tau_\beta$, where ω_c is the cyclotron frequency at $P1$ and τ_β is the characteristic scattering time for ballistic transport in the antidot lattice. The scattering time τ_β was then calculated using $P1 \sim \exp(-2\pi/\omega_c\tau_\beta)$[3]. Since the proportionality factor is not known, the relation allows us to calculate the temperature dependence of the scattering rate $1/\tau_\beta$ only to within a constant, namely its value at $T=0.4$ K. Yet, it is the temperature dependence of $1/\tau_\beta$ that is of interest, and thus Fig. 3 contains this quantity compared to its value at $T=0.4$ K, $\Delta(1/\tau_\beta) = 1/\tau_\beta(T) - 1/\tau_\beta(T=0.4\ \mathrm{K})$ versus T. Figure 3 reveals a linear dependence of $1/\tau_\beta$ on T. For comparison, the inset in Fig. 3 contains the temperature dependence of the mobility scattering rate $1/\tau_\mu$, calculated from μ measured on the plain sample at zero top gate voltage from 0.4 to 152 K. Above 60 K the behavior of $1/\tau_\mu$ approximates $\sim T^2$ while flattening rapidly below 60 K. We interpret the T^2 behavior at such high T as resulting from polar optical phonon scattering, dominant at the higher temperatures.[13] At lower temperatures ($T < \sim 40$ K), temperature independent scattering mechanisms, such as ionized impurity scattering, and interface roughness scattering, limit μ, and result in a constant $1/\tau_\mu$. Optical phonon scattering, however, remains important down to a lower T than in GaAs-based heterostructures, since the longitudinal optical phonon energy in InSb is 24 meV, compared to 36 meV in GaAs. When N_S is increased by means of a positive front gate voltage (3 and 5 V; upper inset in Fig. 3), μ increases and maintains a similar dependence on T. From the increase in μ with N_S at low T, we can conclude that μ is not limited by interface roughness scattering at the lowest temperatures.[14] This leaves ionized impurity and defect-related[15] scattering as the most likely scattering mechanisms determining μ at low T. In contrast to $1/\tau_\mu$, the ballistic scattering rate $1/\tau_\beta$ follows a linear temperature dependence for $0.4\ \mathrm{K} < T < 51\ \mathrm{K}$ (Fig. 3). The linear dependence may result from acoustic phonon scattering. Indeed, at low T, acoustic phonons produce small-angle scattering, to which $1/\tau_\mu$ is not sensitive.[10–12] The ballistic transport measurement, however, is expected to display an enhanced sensitivity to small angle scattering, and may indeed be limited by acoustic phonon scattering at low T. In particular, small-angle scattering has been invoked to explain reduced peak amplitudes in periodically modulated 2DESs.[16]

In summary, we fabricated and measured transport properties of antidot lattices on an InSb/InAlSb heterostructure. Strong characteristic features of ballistic transport were observed at temperatures up to 50 K, beyond which the strictly two-dimensional character of the electron system was lost. The temperature dependence of the magnetotransport data reveals that different scattering mechanisms determine mobility values and ballistic antidot lattice transport features.

The authors acknowledge support from the National Science Foundation under Grant No. DMR-0094055.

[1] K. Ensslin and P. M. Petroff, Phys. Rev. B **41**, 12307 (1990); D. Weiss, M. L. Roukes, A. Menschig, P. Grambow, K. von Klitzing, and G. Weimann, Phys. Rev. Lett. **66**, 2790 (1991).
[2] D. Weiss, K. Richter, E. Vasiliadou, and G. Lütjering, Surf. Sci. **305**, 408 (1994).
[3] J. Heremans, B. K. Fuller, C. M. Thrush, and V. Bayot, Phys. Rev. B **54**, 2685 (1996).
[4] A. Dorn, M. Sigrist, A. Fuhrer, T. Ihn, T. Heinzel, K. Ensslin, W. Wegscheider, and M. Bichler, Appl. Phys. Lett. **80**, 252 (2002).
[5] K. J. Goldammer, S. J. Chung, W. K. Liu, M. B. Santos, J. L. Hicks, S. Raymond, and S. Q. Murphy, J. Cryst. Growth **201/202**, 753 (1999); S. J. Chung, N. Dai, G. A. Khodaparast, J. L. Hicks, K. J. Goldammer, F. Brown, W. K. Liu, R. E. Doezema, S. Q. Murphy, and M. B. Santos, Physica E (Amsterdam) **7**, 809 (2000).
[6] H. Chen, J. J. Heremans, J. A. Peters, J. P. Dulka, A. O. Govorov, N. Goel, S. J. Chung, and M. B. Santos (unpublished); N. Goel, S. J. Chung, M. B. Santos, K. Suzuki, S. Miyashita, and Y. Hirayama, Physica E (Amsterdam) **20**, 251 (2004); **21**, 761 (2004).
[7] J. Eroms, M. Zitzlsperger, D. Weiss, J. H. Smet, C. Albrecht, R. Fleischmann, M. Behet, J. De Boeck, and G. Borghs, Phys. Rev. B **59**, R7829 (1999).
[8] R. Fleischmann, T. Geisel, and R. Ketzmerick, Phys. Rev. Lett. **68**, 1367 (1992).
[9] O. Yevtushenko, G. Lütjering, D. Weiss, and K. Richter, Phys. Rev. Lett. **84**, 542 (2000).
[10] P. C. van Son, H. van Kempen, and P. Wyder, Phys. Rev. Lett. **58** 1567 (1987); J. Spector, H. L. Stormer, K. W. Baldwin, L. N. Pfeiffer, and K. W. West, Surf. Sci. **228**, 283 (1990); F. Nihey, K. Nakamura, M. Kuzuhara, N. Samoto, and T. Itoh, Appl. Phys. Lett. **57**, 1218 (1990).
[11] J. J. Heremans, M. B. Santos, and M. Shayegan, Appl. Phys. Lett. **61**, 1652 (1992).
[12] P. Ramvall, N. Carlsson, P. Omling, L. Samuelson, W. Seifert, and Q. Wang, Appl. Phys. Lett. **70**, 243 (1997); R. G. Mani and J. R. Anderson, Phys. Rev. B **37**, 4299 (1988); S. Das Sarma and Frank Stern, *ibid.* **32**, 8442 (1985).
[13] K. Hirakawa and H. Sakaki, Phys. Rev. B **33**, 8291 (1986).
[14] H. Sakaki, T. Noda, K. Hirakawa, M. Tanaka, and T. Matsusue, Appl. Phys. Lett. **51**, 1934 (1987).
[15] T. D. Mishima, J. C. Keay, N. Goel, M. A. Ball, S. J. Chung, M. B. Johnson, and M. B. Santos, J. Cryst. Growth **251**, 551 (2003).
[16] P. Bøggild, A. Boisen, K. Birkelund, C. B. Sørensen, R. Taboryski, and P. E. Lindelof, Phys. Rev. B **51**, 7333 (1995).